International Journal of Structural Stability and Dynamics
Vol. 21, No. 5 (2021) 2171002 (11 pages)

DOI: 10.1142/S0219455421710024

On Stability of SDOF Systems with Asymmetric Bi-Linear Hysteresis Subjected to Seismic Excitations

Patricio Quintana Gallo[*,‡] and Rodrigo Meneses[†,§]

[*]*School of Civil Engineering*
Pontificia Universidad Católica de Valparaíso
Brasil 2147, Level 3, Valparaiso, Valparaiso, Chile

[†]*School of Civil Engineering, University of Valparaiso*
General Cruz 222, Level 4, Valparaiso, Valparaiso, Chile
[‡]*quintana.gallo@gmail.com*
[§]*rodrigo.meneses@uv.cl*

Received 7 November 2020
Accepted 6 January 2021
Published 19 February 2021

This technical note presents a numerical study on the stability of single degree of freedom (SDOF) systems with asymmetric bi-linear hysteretic restoring force, subjected to earthquake excitations. The aim is to report: (a) the existence of an unstable behavior in the response of such systems, under a specific ground motion, given small modifications of the yielding conditions of the hysteresis model, and (b) the introduction of a novel three-dimensional graphic visualization of the problem. The modifications of the yielding conditions were introduced via the symmetry-breaking produced by very small variations of the static equilibrium position of the system, equivalent to having an initial position and restoring force different from zero and symmetric yielding. The concise study comprises of nonlinear dynamic analyses of three system cases, one of them with symmetric (reference) and two with asymmetric yielding conditions. The results show that the system presented a stable response and severe ratcheting toward the weakest yielding direction for the symmetric and asymmetric cases, respectively. Differences as large as $\pm 2800\%$ between the asymmetric and reference cases were obtained for the residual displacement of the systems, due to variations as small as $\pm 7\%$ in the static-equilibrium position, and consequent $\pm 7\%$ variations of the positive/negative yielding displacements and forces. In turn, negligible variations of the velocity between the three cases were predicted. To conclude, the paper introduces novel three-dimensional representations of the solution-curve and of the hysteresis cycles of the systems, deepening the discussion on the identified bifurcation. The 3D hysteresis curve, in particular, can be of much use for seismic engineering and mechanical studies, either numerical or experimental, as it allows visualizing the sequence of events in the hysteresis plots in a much clearer fashion compared to the traditional two-dimensional counterparts.

Keywords: Single degree of freedom (SDOF) system; asymmetric hysteresis; stability; bifurcation; 3D hysteresis curve; ratcheting.

[‡]Corresponding author.

1. Introduction

Features of the nonlinear dynamic response of single degree of freedom (SDOF) systems with hysteresis have been the subject of qualitative studies covering different aspects of their dependence on the parameters involved in their equation of motion. For specific scenarios, the dynamics of the system can be drastically modified due to small variations of one or more of the parameters fixed in the model. Such scenarios, referred to as "bifurcations" are possible (and expected) due to the nature of the nonlinearity used in the description of the hysteretic restoring force ($H(x)$), and of the external loading ($F(t)$).[1]

In previous research, the stability of SDOF systems with hysteresis involving piecewise-linear functions or the Buoc-Wen and Masing models, has been broadly studied from a dynamical systems perspective.[2–10] These investigations focus on the long-term (large-time) steady-state response of the system and assume a sinusoidal expression for $F(t)$. Several characteristic behaviors of these systems have been reported, including the occurrence of ratcheting, understood as an increasing deviation of the position of the system from its initial value.[9] Such a phenomenon has been associated to features of the system such as an asymmetry in the yielding conditions of the restoring force.[10]

When dealing with earthquake actions, however, the relatively small duration and the erratic (yet bounded) nature of the motion, which can hardly be represented by a single sinusoidal function, render the development of a classical steady-state response not possible. To date, several studies have investigated the seismic response of SDOF with hysteresis, focusing on their residual displacements (x_r),[11–15] and on the existence of ratcheting.[16] The comprehensive studies presented in Refs. 13–15 confirmed the influence of the post-yielding and reloading stiffness of $H(x)$ and its overall shape, on the magnitude of x_r, as observed previously.[11,12] Using statistical analyses of the results of nonlinear dynamic analyses (NLDA) of SDOF systems with several hysteresis models subjected to a large number of earthquake records, these references also showed correlations between x_r and different characteristics of the input ground motions and their associated earthquakes. They concluded that large velocity pulses increase residual displacements,[14] but reported large variability in the results correlating x_r with variables such as site conditions, earthquake magnitude, and distance to the source.[15] Ahn *et al.*,[16] in turn, investigated the propensity of several earthquake records in imposing ratcheting over symmetric bi-linear SDOF systems, concluding that the "likelihood of ratcheting" of a ground motion mostly depends on local site conditions, and the magnitude of the earthquake producing them.

This work addresses the case of SDOF systems with bi-linear hysteresis with asymmetric positive/negative yielding conditions, and post-yielding stiffness equal to zero ($r = 0$), subjected to a single earthquake record. The main purpose is to report the existence of strong dependence of the displacement response of the system on small variations of the yielding conditions of $H(x)$, indirectly introduced by small modification of the static equilibrium conditions, for all other conditions fixed.

These modifications, in turn, can result from the action of a permanent load (F_p) in the direction of motion. The investigation shows that small asymmetries in the positive/negative yielding displacement/force provide favorable conditions for the development of ratcheting in the system, leading to large residual displacements. To further understand and discuss qualitative aspects of the response of the system, this contribution introduces novel three-dimensional (3D) representations of: (1) the displacement–velocity solution curve and (2) the force-displacement hysteresis loops, as explicit functions of the time.

2. Problem Statement and Mathematical Modeling

Figure 1(a) presents a schematic of a SDOF system subjected to the horizontal ground acceleration $a_g(t)$. The system has a symmetric bi-linear restoring force $H(x)$ (Fig. 1(b)). Figure 1(c), in turn, presents the same system defined in Fig. 1(a), but with an added permanent load, F_p, oriented in the direction of motion. Although the model for $H(x)$ is the same for both cases, F_p changes the static equilibrium of the system (initial position and restoring force). If the motion of the system is referred to such condition, the yielding limits of $H(x)$ are altered, breaking its symmetry. Hence, the system is equivalent to that presented in Fig. 1(a), but with asymmetric restoring force $\hat{H}(z)$, as explained next.

The equation of motion of a SDOF system subjected to an external force $F(t)$ can be written as in Eq. (1), where $H(x, \alpha_1, \alpha_2, \ldots, \alpha_m)$ denotes the hysteretic operator used for describing the restoring force, and $\alpha_1, \alpha_2, \ldots, \alpha_m$ are the parameters involved in its formulation. For simplicity, the notation $H(x, \alpha_1, \alpha_2, \ldots, \alpha_m) = H(x)$ is used assuming an implicit dependence on the parameters. In the case of the reference system (Fig. 1(a)), $F(t) = -ma_g(t)$, and the yielding forces of $H(x)$ are $F_y^+ = |F_y^-| = F_y$ (Fig. 1(b)), leading to Eq. (2):

$$m\ddot{x} + c\dot{x} + H(x, \alpha_1, \alpha_2, \ldots, \alpha_m) = F(t), \quad x(0) = x_0; \quad \dot{x}(0) = 0, \tag{1}$$

$$m\ddot{x} + c\dot{x} + H(x) = -ma_g(t), \quad x(0) = 0; \quad \dot{x}(0) = 0. \tag{2}$$

If a permanent load $F_p \neq 0$ is added to the reference system (Fig. 1(b), "loaded" system), in the direction of motion, the conditions of the problem change as follows: (a) the external forcing is $F(t) = -ma_g(t) + F_p$; (b) the initial displacement

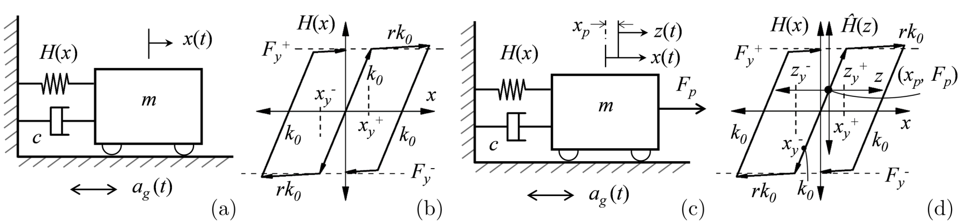

Fig. 1. (a) Reference system with $F_p = 0$; (b) symmetric bi-linear hysteresis for case in (a); (c) system with permanent load $F_p \neq 0$; (d) asymmetric bi-linear hysteresis for case in (c) referred to static equilibrium.

is $x(0) = x_p = F_p/k_0$; and (c) per equilibrium, $H(x_p) = F_p$. Hence, for the loaded system, Eq. (3) holds. Consider the variable $z = x - x_p$, which refers the motion of the mass to the position of static equilibrium. Replacing z and its time derivatives into Eq. (3), Eq. (4) is obtained:

$$m\ddot{x} + c\dot{x} + H(x) = -ma_g(t) + H(x_p), \quad x(0) = x_p; \quad \dot{x}(0) = 0, \tag{3}$$

$$m\ddot{z} + c\dot{z} + H(z + x_p) - H(x_p) = -ma_g(t), \quad z(0) = 0; \quad \dot{z}(0) = 0. \tag{4}$$

In the linear range, it holds that $H(z + x_p) - H(x_p) = H(z)$. However, as there is a change in the reference position, the yielding limits of the hysteresis rule must be adjusted accordingly. This is, formally, the restoring force $\hat{H}(z) = H(z + x_p) - H(x_p)$, with yielding conditions $\hat{H}(z_y^+) = H(x_y^+) - H(x_p)$, and $\hat{H}(z_y^-) = H(x_y^-) - H(x_p)$, must be introduced ($z_y^{\pm} = x_y^{\pm} - x_p$) (see Fig. 1(d)). Replacing this term in Eq. (4), the dynamics of the system are described by Eq. (5). Equation (5) shows how a loaded system with symmetric bi-linear hysteresis is analogous to the reference case with an asymmetric bi-linear hysteresis, if referred to its position of static equilibrium (Fig. 1(d)), provided that $F_y^- < F_p < F_y^+$:

$$m\ddot{z} + c\dot{z} + \overset{\frown}{H}(z) = -ma_g(t), \quad z(0) = 0; \quad \dot{z}(0) = 0. \tag{5}$$

As $H(x)$ is piecewise-linear, the classical results of ordinary differential equations can be applied on each branch. Due to the nature of the nonlinearity of $H(x)$, small variations of the parameters of the system can generate a set of small differences in the local behaviors of the response $x(t)$, which are accumulated in $H(x)$. These differences can lead to large dissimilarities in the solution curve $t \to [t, x(t)]$, producing bifurcations, e.g. with respect to the residual position.[1] This behavior also applies to the hysteresis curve $t \to [x(t), H((x(t))]$, and the three-dimensional plots $t \to [x(t), v(t), t]$, (with $v(t) \equiv \dot{x}(t)$), and $t \to [x(t), H((x(t)), t]$.

3. Definition of Parameters and Analysis Cases

For the reported examples, the parameters of the system were: (1) initial stiffness $k_0 = 8825\,\text{kN/m}$; (2) yielding force $F_y = 750\,\text{kN}$, and, accordingly, yielding displacement $x_y = F_y/k_0 = 85\,\text{mm}$; and (3) mass $m = 235\,\text{ton}$. Consequently, the natural period of vibration of the system is $T = 1.06\,\text{s}$. For the loaded cases, $F_p = 50\,\text{kN} = 0.07\ F_y$, was used. For this force, $x_p \approx 6\,\text{mm}$, 7% of the reference yielding displacement x_y. The viscous damping ratio was taken as $\xi = 5\%$. Table 1 presents the values of the yielding and static equilibrium conditions of the

Table 1. Definition of cases studied (forces in kN and displacements in mm).

Case	F_y^+	F_y^-	x_y^+	x_y^-	F_p^-	x_p	F_p/F_y and x_p/x_y
BL1	750	−750	85	85	0.0	0	0
BL2	700	−800	79	−91	50	6	0.07
BL3	800	−700	91	−79	−50	−6	−0.07

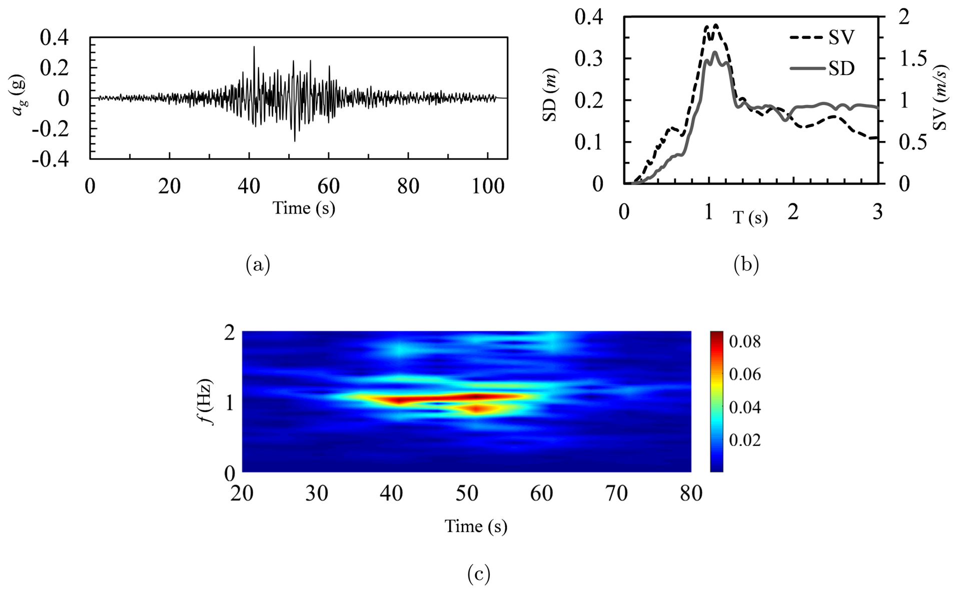

Fig. 2. (a) Acceleration ground motion; (b) displacement and velocity spectra ($\xi = 5\%$); (c) STFT spectrogram.

asymmetric and reference cases. All the numerical results were obtained with the computer program Ruaumoko2D.[17] The numerical scheme consisted of a variation of the Newmark method, which includes iterations with the Newton–Raphson method for identifying the points where $H(x)$ changes branches.[17] The selected input motion was the E–W component of the ground motion recorded during the 2010 Maule earthquake at Marga–Marga station, located in Viña del Mar, Chile. Figure 2 presents the acceleration earthquake record, its linear-elastic displacement and velocity response spectra for $\xi = 5\%$, and the Short-Time Fourier Transform (STFT) spectrogram,[18] which depicts largely predominant frequencies of the motion close to $f = 1\,\text{Hz}$ ($T = 1\,\text{s}$) during its strong part ($|a_g| > 0.1\,\text{g}$, approx).

4. Results

Table 2 summarizes the maximum/minimum amplitudes of x and v ($x_{\max}$, $x_{\min}$, $v_{\max}$, $v_{\min}$), x_r, and the peak and residual displacement ductility factors ($\mu_{\min}$, $\mu_{\max}$, μ_r).

Table 2. Summary of results (displacements in mm; velocities in mm/s; relative error in %).

Case	$x_{\max}$	$Ex_{\max}$	$x_{\min}$	$Ex_{\min}$	$v_{\max}$	$Ev_{\max}$	$v_{\min}$	$Ev_{\min}$	x_r	Ex_r	$\mu_{\max}$	$\mu_{\min}$	μ_r
BL1	149	—	−123	—	789	—	−735	—	13	—	1.8	−1.4	0.2
BL2	459	208	−91	−26	830	5	−717	−2	379	2815	5.4	−1.1	4.5
BL3	84	−44	−431	250	744	−6	−769	5	−352	−2808	1.0	−5.1	−4.1

Table 2 also presents the relative error between the values of $x_{\max}$, $x_{\min}$, $v_{\max}$, $v_{\min}$, and x_r obtained with the asymmetric models with respect to the reference case.

Figure 3 presents the displacement (x) and velocity ($\dot{x} \equiv v$) responses for the three cases defined in Table 1, and their relative asymmetric-to-reference differences in time. Figure 3(a) shows that the $x(t)$ responses obtained with the three cases differ by a large extent, and reveal instability of the displacement response with respect to symmetry-breaking in the yielding conditions of $H(x)$, for the particular conditions of the example (input motion, numerical values of r, m, k_0, ξ). The $x(t)$ response obtained for case BL1 could be considered "stable", with ductility levels of $\mu = 1.8$ or less, and a non-excessive residual displacement, corresponding to $\mu_r = 0.3$.

The displacement histories obtained for cases BL2 and BL3, in turn, present increasing displacements towards the direction with the weakest yielding condition.

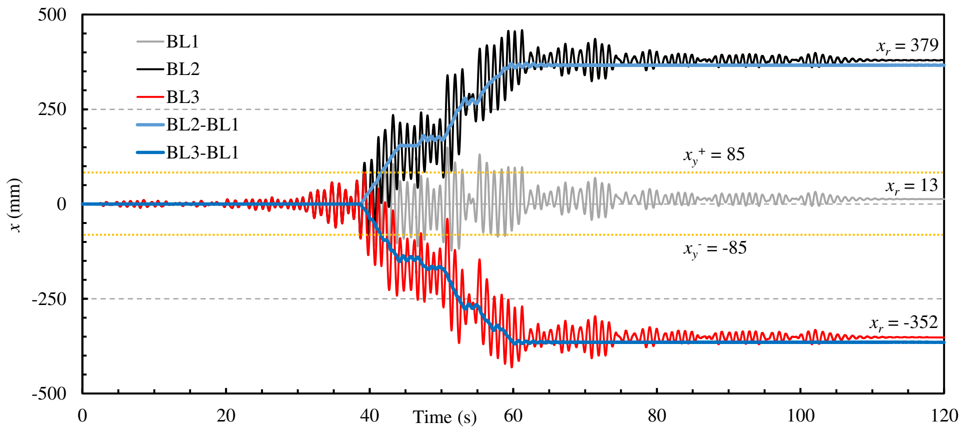

(a)

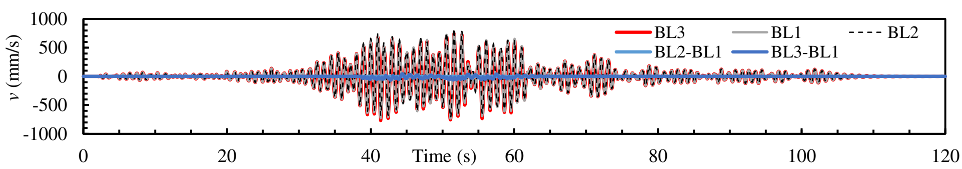

(b)

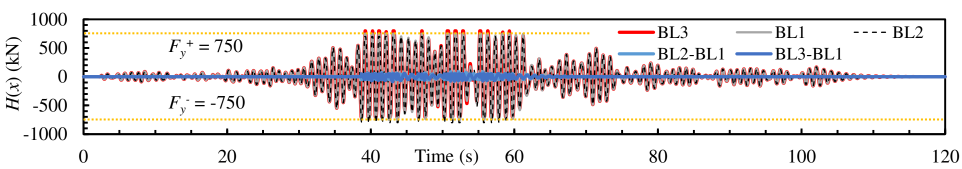

(c)

Fig. 3. Response histories: (a) displacement; (b) velocity; (c) restoring force.

The maximum displacements obtained for these cases correspond to large ductility levels of 5.4 and −5.1, for cases BL2 and BL3, respectively. The residual ductility, in turn, was 4.5 and −4.1 for cases BL2 and BL3, respectively, implying excessively great inelastic permanent deflections. On the other hand, as shown in Fig. 3(b), the velocity responses obtained for the three cases were almost identical. As summarized in Table 2, whilst the maximum displacement errors between cases BL2 and BL3 and the reference case BL1 are as large as 208% and 350%, respectively, the relative differences in the residual displacements are much greater, reaching 2815% and −2808%, respectively. The plots of $H(x(t))$ (Fig. 3(c)), in turn, depict the very small differences between the asymmetric and reference yielding forces.

Figure 4(a) presents the plots of the vector $[x,\, v]$ (also known as phase-portraits[1]) for the three cases, depicting in one single graph how the displacements of the systems BL2 and BL3 present a much larger amplitude towards the weakest direction of $\hat{H}(x)$, while their velocities remain almost identical. Figure 4(b) presents plots of $[x,\, H(x)]$, as commonly done in seismic engineering studies. The plots depict how the loaded systems increase their displacements towards the weakest direction, but without the greatest clarity due to overlapping of the loops.

As the term $F(t) = -ma_g(t)$ depends explicitly on the time, Eq. (2) is a non-autonomous system, implying that $[x,\, v]$ and $[x,\, H(x)]$ are self-intersecting, and thus, not totally satisfactory, from a graphical perspective, for qualitative analyses. As the solution curve $[x,\, v,\, t]$ solves this auto-intersection problem, the dynamics of the restoring force can be qualitatively analyzed considering the curve $[x,\, H(x),\, t]$ and $[x,\, \hat{H}(x),\, t]$ for the reference and asymmetric systems, respectively. Figure 5(a) shows, more clearly, the bifurcation scenario developing when the symmetry of the yielding conditions is broken. The graphs also show how the velocity of the three systems are very similar, with small differences arising during the ratcheting part of the motion. Figure 5(b), in turn, shows how the large hysteresis cycles developed from $t = 38.7$ s, when inelasticity takes place for the first time. This shape, which resembles an 'inverted cascade' due to its evolution in time, unveils valuable qualitative/graphical information which is magnified in Fig. 6.

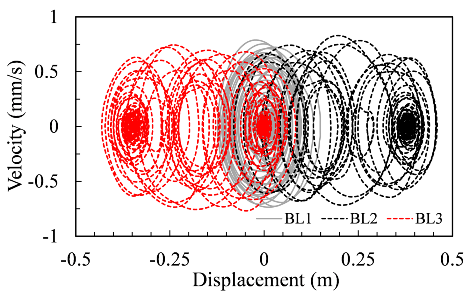

(a)

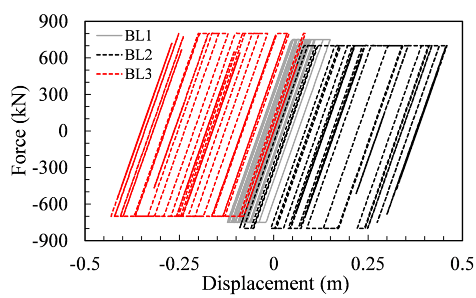

(b)

Fig. 4. (a) 2D phase plots $[x,\, v]$; (b) 2D hysteresis plots $[x,\, H(x)]$.

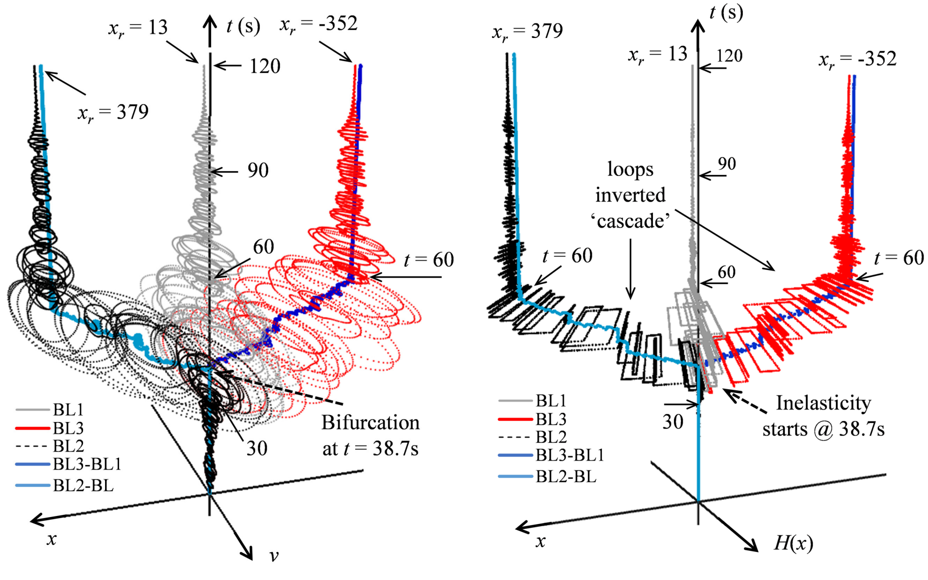

Fig. 5. Novel 3D diagrams: (a) solution-curves $[x,\, v,\, t]$; (b) hysteresis curves $[x,\, H(x),\, t]$.

Figure 6(a), presenting the curves $[x,\, H(x),\, t]$ and $[x,\, \hat{H}(x),\, t]$ for cases BL1 and BL2, respectively, shows that the position of the system BL2 displaces towards the direction with the weakest yielding condition (x_y^+) between $t = 38.7$ s and $t = 60$. This time interval approximately coincides with the strong part of the input

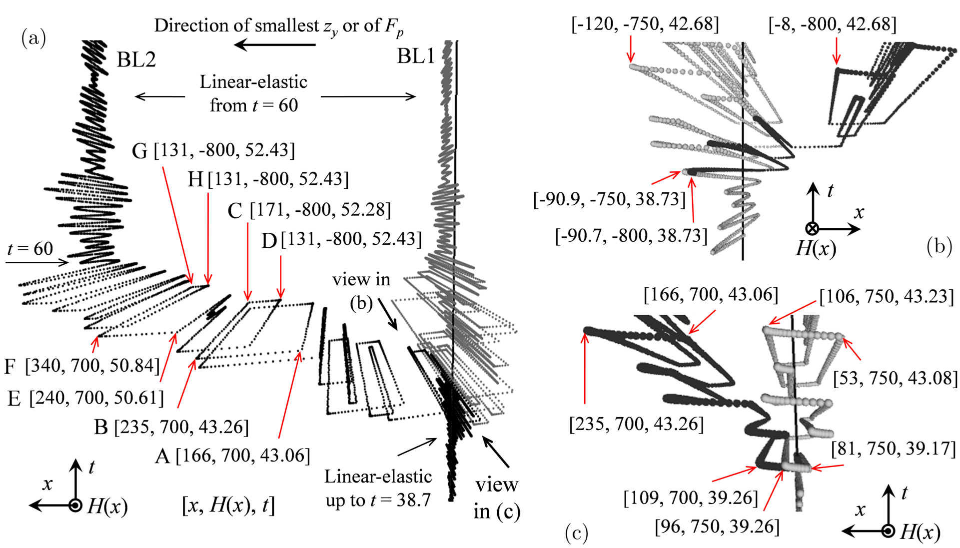

Fig. 6. BL1 and BL2 3D hysteresis close-up: (a) strong part of motion; (b) and (c) views indicated in (b).

motion, characterized by large STFT values close to $f = 1\,\text{Hz}$ (Fig. 2). As the natural frequency of the system is $f_0 = 0.93\,\text{Hz}$, the responses might be influenced by resonance. The ratcheting behavior obtained for cases BL2 and BL3 is produced by accumulation of the differences between the inelastic displacements reached in the $\pm$ directions during several individual hysteresis cycles. The coordinates of the points A to K in Fig. 6(a) depict how the difference in x cumulates towards the positive direction during three inelastic cycles of the response, including some oscillation in the linear range in F-G-H. The lengths of the positive branches AB, EF, and HI are larger than those of the negative counterpart branches CD, GG, and JK. The branch GG, in turn, denotes that no inelastic incursion occurred in the negative direction prior to yielding taking place in the positive direction again (point H).

Figure 6(b) provides insight into the conditions of the response of cases BL1 and BL2 around the time when the differences in their responses begin (points A_1 and A_2). Figure 6(b) also identifies the points L_1 and L_2 in the response of BL1 and BL2, respectively, where the largest inelastic displacement in the negative direction of a local hysteresis cycle is reached in both models. The displacements of the systems associated to L_1 and L_2, occuring only approximately four seconds after the beginning of the first inelastic incursions, differ by as much as $112\,\text{mm}$ ($\mu = 1.3$), as a result of the sequence of hysteresis cycles with larger displacements in the positive post-yielding branches of $\hat{H}(x)$ compared to the negative. Finally, Fig. 6(c) presents the plots in Fig. 6(b) from the opposite perspective. The points B_1 and B_2 correspond to those where inelasticity is firstly reached in the positive direction, whereas the points C_1 and C_2 indicate the end of such incursions. Using the coordinates in these points, and those of A_1 and A_2, it is found that the post-elastic branch in the first cycle of BL2 is equal to $27.9\,\text{mm}$ ($\mu = 0.33$), depicting how larger positive than negative post-elastic displacements within individual loops arise in such systems from the first inelastic cycle onward.

5. Summary and Conclusions

As series of NLDA were carried out to study the stability of the response of a SDOF system with bi-linear hysteretic restoring force, $H(x)$, due to small modifications of its yielding conditions. These modifications are included by breaking the symmetry of the positive/negative yielding force/displacement of the backbone curve of $H(x)$, resulting from very small variations of the static equilibrium position of the system, e.g. caused by small permanent loads acting in the direction of motion. The study comprised of three system cases, one of them with symmetric and two with asymmetric yielding conditions. The results of the NLDA showed the existence of large differences in the responses obtained with the reference and asymmetric (loaded) systems. Whilst the reference system presented a stable displacement-response with minor residual displacement (x_r), the asymmetric systems presented ratcheting toward the direction of the smallest yielding displacement (weakest yielding force) of

$H(x)$, with x_r 28 times (2800%) larger than that for the reference case. The velocity-responses, in turn, were almost identical for all cases, with asymmetric/reference variation of the maximum amplitude of 10% or less. By means of 3D representations of $[x(t), v(t), t]$, and particularly of $[x(t), H(x(t)), t]$, introduced in the paper, a novel framework was developed for the graphical study of a bifurcation scenario associated to the evaluation of the stability of SDOF with hysteresis. The 3D representation of the hysteresis allowed decomposing the dynamics of the systems in different intervals of time containing individual hysteresis loops, which helped visualizing how, in the asymmetric cases, the differences in the inelastic displacements with opposite sign within individual cycles accumulate towards the direction of the weakest yielding condition, producing large residual displacements. The proposed 3D plot of the hysteresis can be of much use for engineering studies involving such a phenomenon, as it clearly depicts the evolution of $H(x)$ in time, sorting out the self-intersection problems presented by traditional 2D hysteresis plots.

Acknowledgement

The time provided by BRANZ Ltd. (New Zealand) for scoping this work and the comments of several of its staff members are much appreciated. Special thanks to Andries Labuschagne and Suzanne Lester for gathering part of the reference material during the scoping period. The support of the students of the School of Civil Engineering of the University of Valparaíso, where part of this work was carried out, is gratefully acknowledged.

References

1. Y. A. Kuznetsov, *Elements of Applied Bifurcation Theory* (Springer, New York, NY, 1998).
2. T. K. Caughey, Sinusoidal excitation of a system with bilinear hysteresis, *J. Appl. Mech.* **27** (1960) 649–652.
3. D. Capecchi and F. Vestroni, Steady-state dynamic analysis of hysteretic systems, *J. Eng. Mech.* **111** (1985) 1515–1531.
4. N. Challamel and G. Gilles, Stability and dynamics of a harmonically excited elastic-perfectly plastic oscillator, *J. Sound Vib.* **301** (2007) 608–634.
5. T. Kalmár-Nagy and A. Shekhewat, Nonlinear dynamics of oscillators with bilinear hysteresis and sinusoidal excitation, *Physica D* **238** (2009) 1768–1786.
6. W. Lacarbonara and F. Vestroni, Nonclassical response of oscillators with hysteresis, *Nonlinear Dyn.* **32** (2003) 235–258.
7. G. Miller and M. Butler, Periodic response of elasto-perfectly plastic SDOF oscillator, *J. Eng. Mech.* **3** (1998) 536–550.
8. S. W. Shaw and P. J. Holmes, A periodically forced piecewise-linear oscillator, *J. Sound Vib.* **90** (1983) 129–155.
9. I. Ahn, S. Chen and G. Dargush, An iterated maps approach for dynamical ratcheting in SDOF hysteretic damping systems, *J. Sound Vib.* **323** (2009) 896–909.
10. N. Challamel, C. Lanos, A. Hammouda and B. Redjel, Stability analysis of dynamic ratcheting in elastoplastic systems, *Phys. Rev. E* **75** (2007) 026204.

11. G. MacRae and K. Kawashima, Post-earthquake residual displacements of bilinear oscillators, *Earthquake Eng. Struct. Dyn.* **26** (1997) 701–716.
12. C. Christopoulos, S. Pampanin and M. J. N. Priestley, Performance-based seismic response of frame structures including residual deformations. Part I: Single-degree of freedom systems, *J. Earthquake. Eng.* **7** (2003) 97–118.
13. E. Liossatou and M. Fardis, Near-fault effects on residual displacements of RC structures, *Earthquake Eng. Struct. Dyn.* **45** (2016) 1391–1409.
14. E. Liossatou and M. Fardis, Residual displacements of RC structures as SDOF systems, *Earthquake Eng. Struct. Dyn.* **44** (2015) 713–734.
15. J. Ruiz-Garcia and E. Miranda, Residual displacement ratios for assessment of existing structures, *Earthquake Eng. Struct. Dyn.* **35** (2006) 315–336.
16. I. Ahn, S. Chen, G. Dargush and L. Cheng, Dynamic ratcheting in SDOF hysteretic damping systems induced by earthquake excitations, *Eng. Struct.* **100** (2015) 665–673.
17. A. J. Carr, *Ruaumoko: Computer Program for Inelastic Dynamic Analysis. Volume 1: Theory* (Carr Research Ltd., Christchurch, New Zealand, 2016).
18. H. Zhivomirov, On the development of STFT-analysis and ISTFT-synthesis routines and their practical implementation, *TEM J.* **8** (2019) 56–64.